Construction of Advanced S-Scheme Heterojunction Interface Composites of Bimetallic Phosphate $MnMgPO_4$ with C_3N_4 Surface with Remarkable Performance in Photocatalytic Hydrogen Production and Pollutant Degradation

Ting Cheng [1,2,3], Jiarui Zhu [3], Chen Chen [3,*], Yulin Hu [4], Liangliang Wu [3], Mengyi Zhang [3], Liwei Cui [3], Youzhi Dai [5], Xiao Zhang [1,2,6], Yuan Tian [3] and Fei Wu [3]

1 School of Environmental Ecology, Jiangsu City Vocational College, Nanjing, 210017, China; wnchengting@sina.com (T.C.); zhangxiao7376@sina.com (X.Z.)

2 Jiangsu Engineering and Technology Centre for Ecological and Environmental Protection in Urban and Rural Water Environment Management and Low Carbon Development, Nanjing 210017, China

3 School of Environmental and Chemical Engineering, Jiangsu University of Science and Technology, Zhenjiang 212100, China; zjr000323@163.com (J.Z.); w18852913906@163.com (L.W.); zhangmengyi031029@163.com (M.Z.); cui36984628@163.com (L.C.); ttyy1974.ok@163.com (Y.T.); wufei1224wf@hotmail.com (F.W.)

4 College of Chemistry and Chemical Engineering, Anshun University, Anshun 561000, China; huyulin1982@163.com

5 College of Environment and Resource, Xiangtan University, Xiangtan 411105, China; daiyouzhi202@163.com

6 Nanjing University and Yancheng Academy of Environmental Technology and Engineering, Yancheng 224000, China

* Correspondence: chenc@just.edu.cn

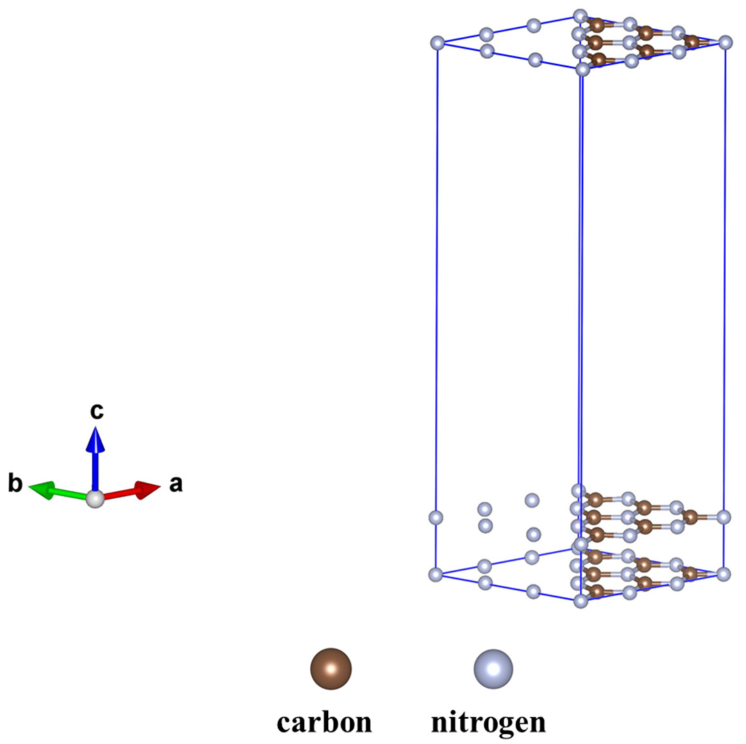

Figure S1. DFT theoretical work function calculation models of C_3N_4.

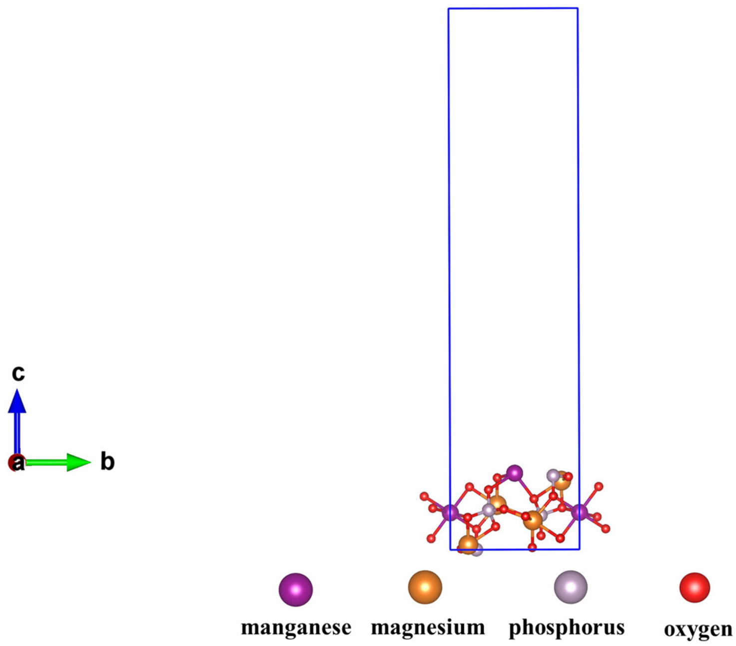

Figure S2. DFT theoretical work function calculation models of MgMnP.

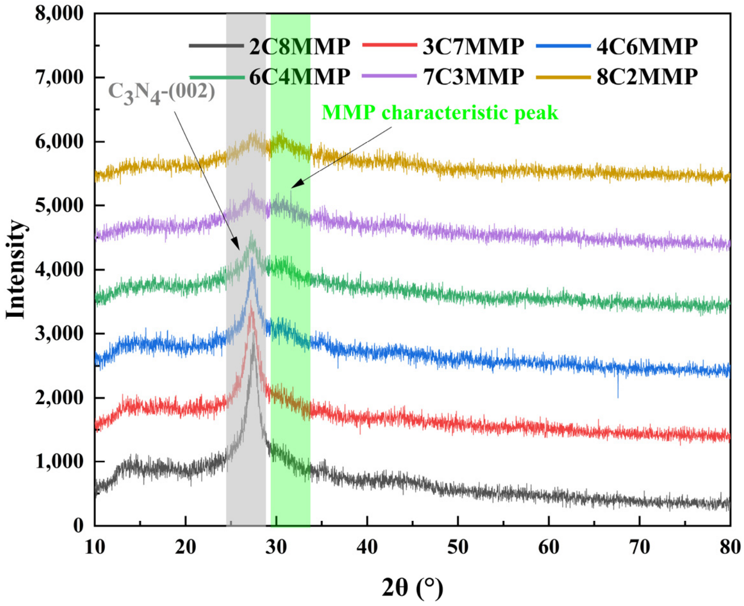

Figure S3. The XRD patterns of composite materials with different C_3N_4 and MgMnP ratios.

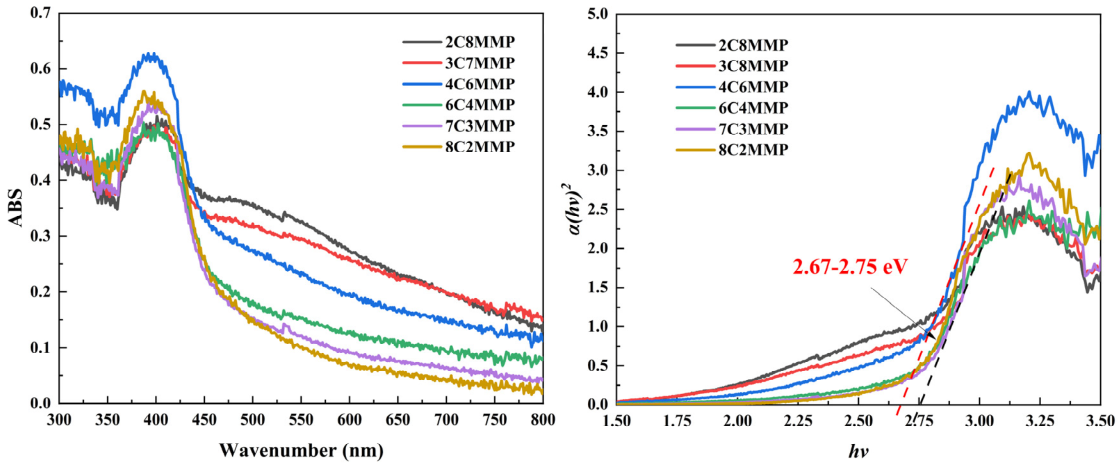

Figure S4. The UV-Vis diffuse reflectance spectra (a) and band fitting results (b) of composite materials with different C_3N_4 and MgMnP ratios.

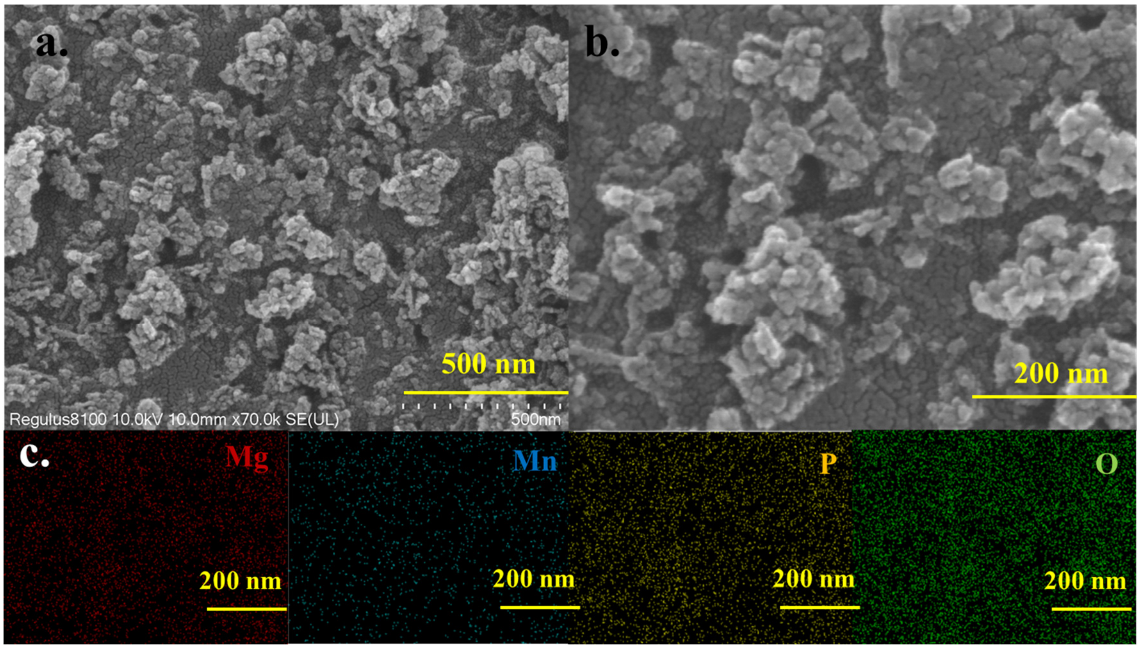

Figure S5. The SEM morphology analysis results of MgMnP material (a and b); the SEM-EDX elemental mapping analysis results of MgMnP material (c).

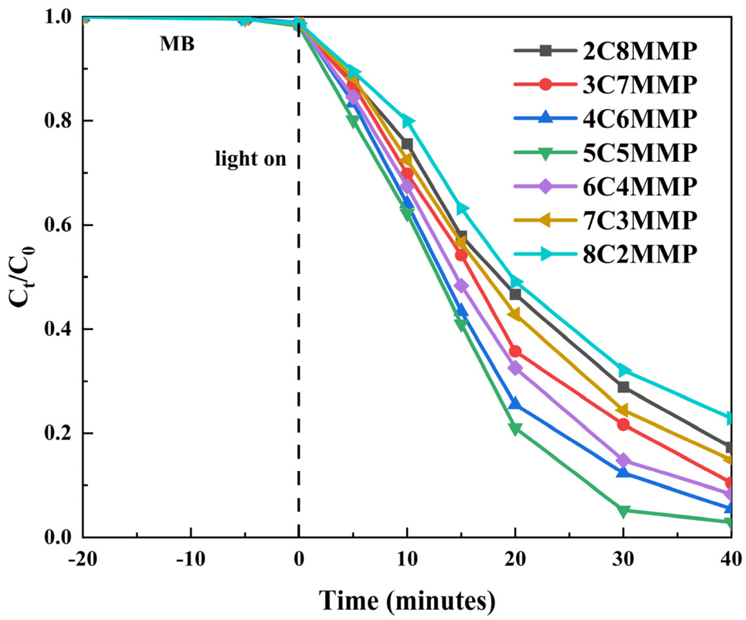

Figure S6. The photocatalytic degradation curves of MB using composites with different C_3N_4 and MgMnP ratios.

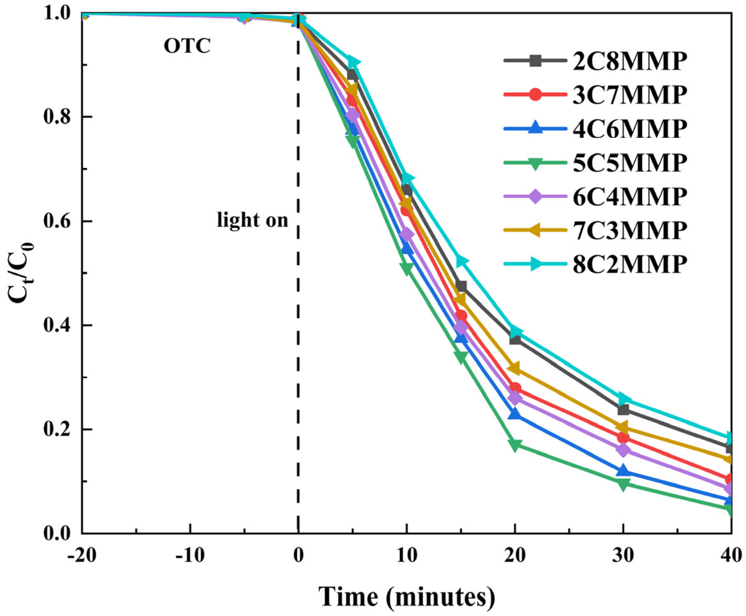

Figure S7. The photocatalytic degradation curves of OTC using composites with different C_3N_4 and MgMnP ratios.

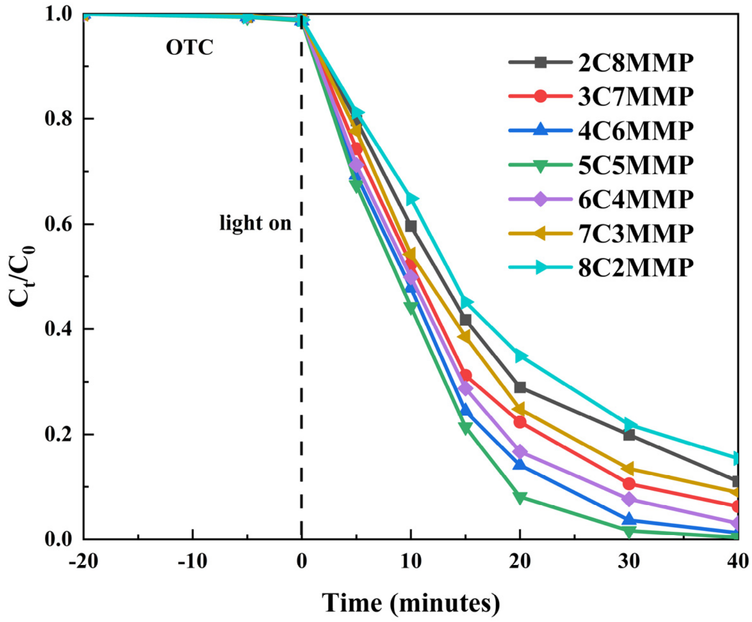

Figure S8. The photocatalytic degradation curves of TE using composites with different C_3N_4 and MgMnP ratios.

Table S1. The photocatalytic degradation efficiency of MB for recent photocatalysts.

Catalyst	Light source	Concentration (mg/L)	Catalyst dosage (mg/ml)	Degradation (%)	Reference
$MgFe_2O_4$	Sunlight	10	20/40	80 (120mins)	[58]
$NiMn_2O_4/ZnMn_2O_4$	200W tungsten lamp	20	10/100	92 (80mins)	[59]
$Ag_3PO_4/MnFe_2O_4$	Sunlight	15	25/50	98 (82mins)	[60]
$Ni_{0.6}Zn_{0.4}Fe_2O_4$	Mercury vapor Lamp	20	30 /100	94 (275mins)	[61]
ZnFe2O4/ZnO	UV lamp	10	100/100	100 (180mins)	[62]
Co/Ni-MOF@BiOI	Sunlight	10	80/100	99 (200mins)	[63]
Ti/TiN/TiON/TiO2	250 W mercury lamp	1	20/20ml	69 (60mins)	[64]
Ag-ZnO/MWCNT	30 W UV lamp	10	24/80	98 (250mins)	[65]
CVCs	40 W white LED	5	50/100	96.2 (80mins)	[66]
MgMnP/C3N4	300W Xe lamp	10	20/30	almost 100 (40mins)	This work

Table S2. The photocatalytic degradation efficiency of OTC for recent photocatalysts.

Catalyst	Light source	Concentration (mg/L)	Catalyst dosage (mg/ml)	Degradation (%)	Reference
CVCs	40 W white LED	20	50/100	80.5 (80mins)	[66]
Co_3O_4/TiO_2/GO	300 W Xe lamp	10	50/200	91 (90mins)	[67]
Bi_2WO_6–BiOCl	500 W Xe lamp	20	30/30	93 (300mins)	[68]
GTZ	Visible 300 W	10	20/100	100 (180mins)	[69]
$H_2O_2/ZnWO_4$/CaO	Sunlight	10	50/50	85 (210min)	[70]
N,Fe-CDs/G-WO_3-0.6	500 W Xe lamp	20	50/50	47.8 (150mins)	[71]
ZZFDT	300 W Xe lamp	10	100/100	95 (150mins)	[72]
(S-TiO_2/WS_2/alginate beads	Sunlight	10	50/100	92. 5 (240mins)	[73]
$BiBaO_3/Ag_3PO_4$	300W Xe lamp	20	20/30	100 (40mins)	[74]
MgMnP/C_3N_4	300W Xe lamp	10	20/30	almost 100 (40mins)	This work

Table S3. The photocatalytic degradation efficiency of TE for recent photocatalysts.

Catalyst	Light source	Concentration (mg/L)	Catalyst dosage (mg/ml)	Degradation (%)	Reference
CVCs	40 W white LED	40	50/100	86 (80min)	[66]
BiBaO3/Ag3PO4	300W Xe lamp	20	20/30	100 (40mins)	[74]
BTO	300 W Xe UV lamp	40	30/50	64.2 (60mins)	[75]
NiFe-LDH/CTF	300W Xe lamp	40	20/100	85.6 (120mins)	[76]
SrTiO3/TiO2	300W Xe lamp	20	30/25	90 (40mins)	[77]
PCN-5	300W Xe lamp	20	30/100	83.8 (60mins)	[78]
Co-CNK-OH	Sunlight	20	50/100	87.1 (40mins)	[79]
Cr2O3/ZrO2	300W Xe lamp	50	100/100	97.1 (120mins)	[80]
Ce/Bi/BiOCl	300 W Xe arc lamp	40	50/100	97.7 (20mins)	[81]
MgMnP/C3N4	300W Xe lamp	10	20/30	almost 100 (40mins)	This work

Table S4. The kinetic constants of each photocatalytic pollutant degradation system.

MB	
System	Kinetic constant ($minute^{-1}$)
2C8MMP	0.0446
3C7MMP	0.0573
4C6MMP	0.0752
5C5MMP	0.0959
6C4MMP	0.0653
7C3MMP	0.0494
8C2MMP	0.0387
OTC	
System	Kinetic constant ($minute^{-1}$)
2C8MMP	0.0471
3C7MMP	0.0584
4C6MMP	0.0709
5C5MMP	0.0793
6C4MMP	0.0626
7C3MMP	0.0512
8C2MMP	0.0448
TE	
System	Kinetic constant ($minute^{-1}$)
2C8MMP	0.0555
3C7MMP	0.0718
4C6MMP	0.1136
5C5MMP	0.1452
6C4MMP	0.0888
7C3MMP	0.0632
8C2MMP	0.0484

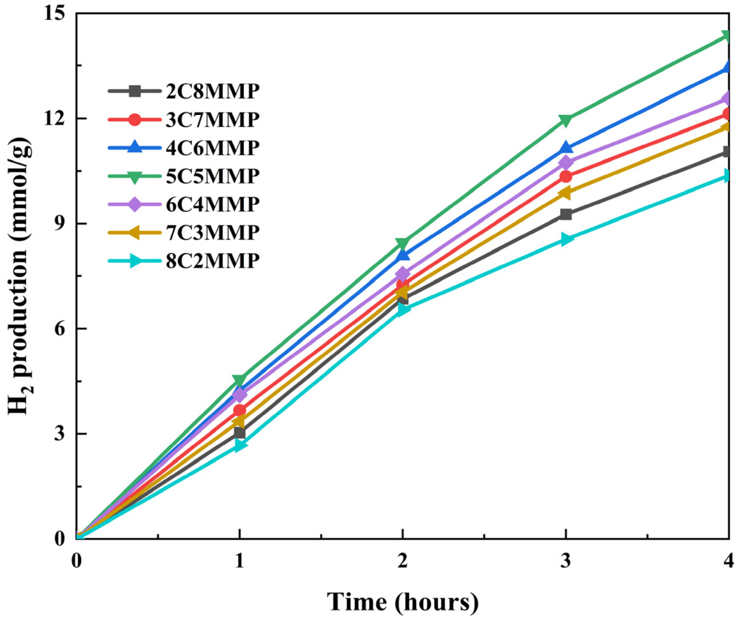

Figure S9. The photocatalytic hydrogen evolution curves of composites with different C_3N_4 and MgMnP ratios.

Table S5. The apparent H_2 production rate constant of each photocatalytic system.

TE	
System	Apparent kinetic constant (mmol·g^{-1}·h^{-1})
2C8MMP	2.764
3C7MMP	3.034
4C6MMP	3.358
5C5MMP	3.595
6C4MMP	3.143
7C3MMP	2.941
8C2MMP	2.592

Table S6. The hydrogen evolution efficiency of recent photocatalysts.

Catalyst	Light source	Apparent H_2 production rate constant (m mol·g^{-1}·h^{-1})	Reference
AgCl/CCN	300 W Xe lamp	0.335	[82]
Cu–Zn0.5Cd0.5S	300 W Xe lamp	1.904	[83]
MoP/a-TiO2/Co-ZnIn2S4	300 W Xe lamp	2.96	[84]
CF/SrTiO 3/CdS	300 W arc lamp	0.578	[85]
WS 2/WSe 2	300 W Xe lamp	3.857	[86]
NiFe2O4/Cu2O	300 W Xe lamp	0.004	[97]
NH2-ZSTU	300 W Xe lamp	0.431	[88]
Bi4Ti3O12/ZnIn2S4	300 W Xe lamp	19.8	[89]
ZnO/Co3O4	350 W Xe lamp	0.793	[90]
MgMnP/C3N4	300W Xe lamp	3.595	This work

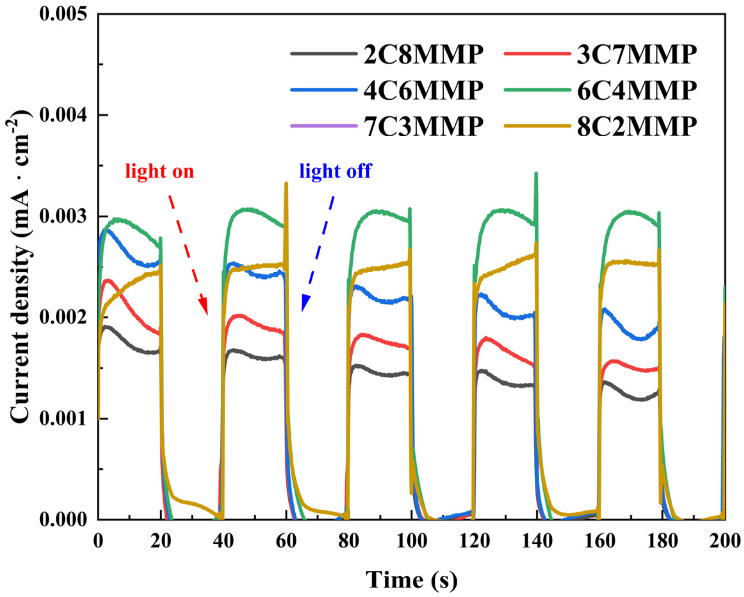

Figure S10. The photocurrent analysis results of 2C8MMP, 3C7MMP, 4C6MMP, 6C4MMP, 7C3MMP, and 8C2MMP composite materials.

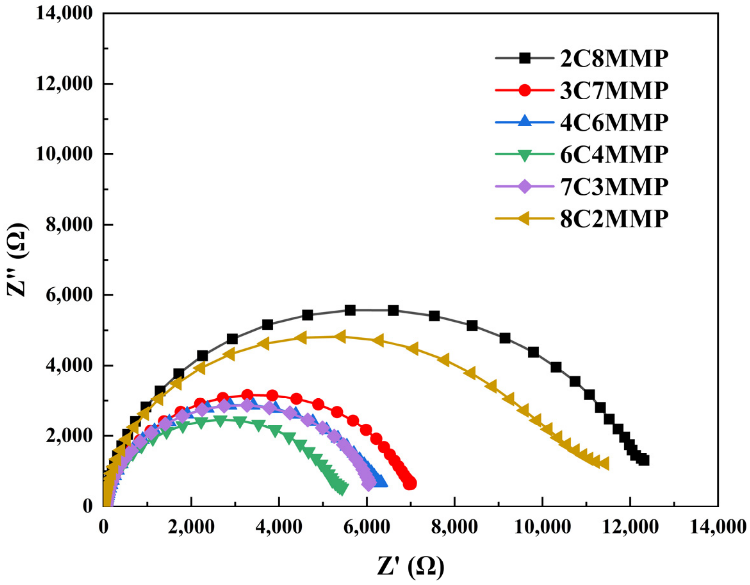

Figure S11. The electrochemical impedance analysis results of 2C8MMP, 3C7MMP, 4C6MMP, 6C4MMP, 7C3MMP, and 8C2MMP composite materials.

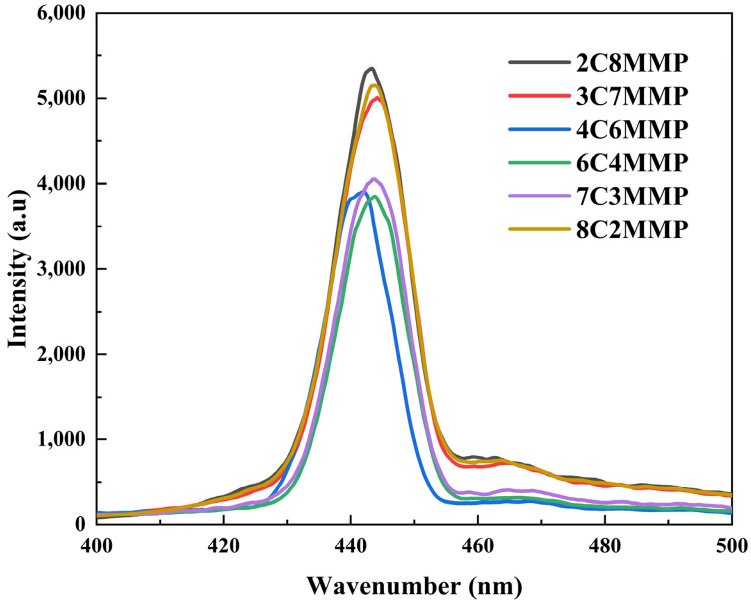

Figure S12. The solid-state fluorescence analysis results of 2C8MMP, 3C7MMP, 4C6MMP, 6C4MMP, 7C3MMP, and 8C2MMP composite materials.

References

[58] HAMMACHE Z, SOUKEUR A, OMEIRI S, BELLAL B, TRARI M. Physical and photo-electrochemical properties of MgFe2O4 prepared by sol gel route: application to the photodegradation of methylene blue [J]. Journal of Materials Science: Materials in Electronics, 2019, 30(6): 5375-5382 doi: https://doi.org/10.1007/s10854-019-00830-2.

[59] FAWY K F, ASHIQ M F, ALHARBI F F, MANZOOR S, NISA M U, IBRAHIM M, KHAN M T N, MESSALI M, CHUGHTAI A H, ASHIQ M N. Facile synthesis of NiMn2O4/ZnMn2O4 heterostructure nanocomposite for visible-light-driven degradation of methylene blue dye [J]. Journal of Taibah University for Science, 2024, 18(1): 2302656 doi: https://doi.org/10.1080/16583655.2024.2302656.

[60] ABROSHAN E, FARHADI S, ZABARDASTI A. Novel magnetically separable Ag3PO4/MnFe2O4 nanocomposite and its high photocatalytic degradation performance for organic dyes under solar-light irradiation [J]. Solar Energy Materials and Solar Cells, 2018, 178: 154-163 doi: https://doi.org/10.1016/j.solmat.2018.01.026.

[61] PADMAPRIYA G, MANIKANDAN A, KRISHNASAMY V, JAGANATHAN S K, ANTONY S A. Spinel Ni Zn1Fe2O4 ($0.0 \leq x \leq 1.0$) nano-photocatalysts: Synthesis, characterization and photocatalytic degradation of methylene blue dye [J]. Journal of Molecular Structure, 2016, 1119: 39-47 doi: https://doi.org/10.1016/j.molstruc.2016.04.049.

[62] SHAO R, SUN L, TANG L, CHEN Z. Preparation and characterization of magnetic core–shell ZnFe2O4@ZnO nanoparticles and their application for the photodegradation of methylene blue [J]. Chemical Engineering Journal, 2013, 217: 185-191 doi: https://doi.org/10.1016/j.cej.2012.11.109.

[63] SIDDIQA A, AKHTER T, FAHEEM M, RAZZAQUE S, MAHMOOD A, AL-MASRY W, NADEEM S, HASSAN S U, YANG H, PARK C H. Bismuth-Rich Co/Ni Bimetallic Metal-Organic Frameworks as Photocatalysts toward Efficient Removal of Organic Contaminants under Environmental Conditions [J]. Micromachines (Basel), 2023, 14(5): 899 doi: https://doi.org/10.3390/mi14050899.

[64] MUSLIMOV A, ORUDZHEV F, GADZHIEV M, SELIMOV D, TYUFTYAEV A, KANEVSKY V. Facile Synthesis of Ti/TiN/TiON/TiO2 Composite Particles for Plasmon-Enhanced Solar Photocatalytic Decomposition of Methylene Blue [J]. Coatings, 2022, 12(11): 1741 doi: https://doi.org/10.3390/coatings12111741.

[65] LóPEZ ALEJANDRO E M, RAMíREZ MORALES E, ARELLANO CORTAZA M C, MORáN LáZARO J P, PéREZ HERNáNDEZ G, ROJAS BLANCO L. Synthesis of Ag-modified ZnO/MWCNT nanoparticles and their application as a catalyst in the degradation of methylene blue [J]. Digest Journal of Nanomaterials and Biostructures, 2023, 18(3): 941-950 doi: https://doi.org/10.15251/djnb.2023.183.941.

[66] FENG J, RAN X, WANG L, XIAO B, LEI L, ZHU J, LIU Z, XI X, FENG G, DAI Z, LI R. The Synergistic Effect of Adsorption-Photocatalysis for Removal of Organic Pollutants on Mesoporous Cu2V2O7/Cu3V2O8/g-C3N4 Heterojunction [J]. International Journal of Molecular Sciences, 2022, 23(22) doi: https://doi.org/10.3390/ijms232214264.

[67] JO W-K, KUMAR S, ISAACS M A, LEE A F, KARTHIKEYAN S. Cobalt promoted TiO2/GO for the photocatalytic degradation of oxytetracycline and Congo Red [J]. Applied Catalysis B: Environmental, 2017, 201: 159-168 doi: https://doi.org/10.1016/j.apcatb.2016.08.022.

[68] GUO M, ZHOU Z, YAN S, ZHOU P, MIAO F, LIANG S, WANG J, CUI X. Bi2WO6-BiOCl heterostructure with enhanced photocatalytic activity for efficient degradation of oxytetracycline [J]. Scientific reports, 2020, 10(1): 18401 doi: https://doi.org/10.1038/s41598-020-75003-x.

[69] HU X-Y, ZHOU K, CHEN B-Y, CHANG C-T. Graphene/TiO2/ZSM-5 composites synthesized by mixture design were used for photocatalytic degradation of oxytetracycline under visible light: Mechanism and biotoxicity [J]. Applied Surface Science, 2016, 362: 329-334 doi: https://doi.org/10.1016/j.apsusc.2015.10.192.

[70] RAIZADA P, SHANDILYA P, SINGH P, THAKUR P. Solar light-facilitated oxytetracycline removal from the aqueous phase utilizing a H2O2/ZnWO4/CaO catalytic system [J]. Journal of Taibah University for Science, 2018, 11(5): 689-699 doi: https://doi.org/10.1016/j.jtusci.2016.06.004.
[71] NI T, LI Q, YAN Y, WANG F, CUI X, YANG Z, WANG Y, YANG Z, CHANG K, LIU G. N,Fe-Doped Carbon Dot Decorated Gear-Shaped WO3 for Highly Efficient UV-Vis-NIR-Driven Photocatalytic Performance [J]. Catalysts, 2020, 10(4): 416 doi: https://doi.org/10.3390/catal10040416.
[72] XUE L, LIANG E, WANG J. Fabrication of magnetic ZnO/ZnFe2O4/diatomite composites: improved photocatalytic efficiency under visible light irradiation [J]. Journal of Materials Science: Materials in Electronics, 2022, 33(3): 1405-1424 doi: https://doi.org/10.1007/s10854-021-07568-w.
[73] KUMAR R, ANSARI M O, TALEB M A, OVES M, BARAKAT M A, ALGHAMDI M A, AL MAKISHAH N H. Integrated Adsorption-Photocatalytic Decontamination of Oxytetracycline from Wastewater Using S-Doped TiO2/WS2/Calcium Alginate Beads [J]. Catalysts, 2022, 12(12): 16776 doi: https://doi.org/10.3390/catal12121676.
[74] ZHANG X, CHEN C, CHENG T, TIAN Y, WEN M, HOU B, XIN X, PAN F, SHI J. Construction highly efficient p–n heterojunctions composite of BiBaO3 and Ag3PO4 for visible light driven photocatalytic degradation of tetracycline and oxytetracycline [J]. Water Resources and Industry, 2024, 31: 100246 doi: https://doi.org/10.1016/j.wri.2024.100246.
[75] GUO Q, GAO T, PADERVAND M, DU D, ZHAO K, ZHANG Y, JIA T, WANG C. Piezo-Photocatalytic Degradation of Tetracycline by 3D BaTiO3 Nanomaterials: The Effect of Crystal Structure and Catalyst Loadings [J]. Processes, 2023, 11(12) doi: https://doi.org/10.3390/pr11123323.
[76] ZHANG J, CHEN X, CHEN Q, HE Y, PAN M, HUANG G, BI J. Insights into Photocatalytic Degradation Pathways and Mechanism of Tetracycline by an Efficient Z-Scheme NiFe-LDH/CTF-1 Heterojunction [J]. Nanomaterials (Basel), 2022, 12(23): 4111 doi: https://doi.org/10.3390/nano12234111.
[77] CHEN W, ZHAO N, HU M, LIU X, DENG B. Strengthened Removal of Tetracycline by a Bi/Ni Co-Doped SrTiO3/TiO2 Composite under Visible Light [J]. Catalysts, 2024, 14(8) doi: https://doi.org/10.3390/catal14080539.
[78] ZHENG K, CHEN J, GAO X, CAO X, WU S, SU J. Photocatalytic degradation of tetracycline by Phosphorus-doped carbon nitride tube combined with peroxydisulfate under visible light irradiation [J]. Water science and technology, 2021, 84(8): 1919-1929 doi: https://doi.org/10.2166/wst.2021.376.
[79] HOU D, LUO J, SUN Q, ZHANG M, WANG J. Preparation of Co-CNK-OH and Its Performance in Fenton-like Photocatalytic Degradation of Tetracycline [J]. Catalysts, 2023, 13(4): 715 doi: https://doi.org/10.3390/catal13040715.
[80] WEI X, NARAGINTI S, CHEN P, LI J, YANG X, LI B. Visible Light-Driven Photocatalytic Degradation of Tetracycline Using p-n Heterostructured Cr2O3/ZrO2 Nanocomposite [J]. Water, 2023, 15(20): 3702 doi: https://doi.org/10.3390/w15203702.
[81] GAO T, CHU H, WANG S, LI Z, ZHOU W. Construction of Ternary Ce Metal-Organic Framework/Bi/BiOCl Heterojunction towards Optimized Photocatalytic Performance [J]. Nanomaterials (Basel), 2024, 14(16): 1352 doi: https://doi.org/10.3390/nano14161352.
[82] JIANG Y, YAN X, FU X, GU Q. Enhanced visible-light-driven co-production of H2 and value-added chemicals over AgCl/crystalline carbon nitride with N defects [J]. Colloid and Interface Science Communications, 2022, 48: 100627 doi: https://doi.org/10.1016/j.colcom.2022.100627.
[83] CHEN H, ZHU Y, WU J, PENG M, DENG S, YANG H, YANG J. Cu-doped ZnCdS-based photocatalyst for efficient photocatalytic hydrogen production by photothermal assistance [J]. Case Studies in Thermal Engineering, 2024, 61 doi: https://doi.org/10.1016/j.csite.2024.104970.

[84] WU K, SHANG Y, LI H, WU P, LI S, YE H, JIAN F, ZHU J, YANG D, LI B, WANG X. Synthesis and Hydrogen Production Performance of MoP/a-TiO2/Co-ZnIn2S4 Flower-like Composite Photocatalysts [J]. Molecules, 2023, 28(11): 4350 doi: https://doi.org/10.3390/molecules28114350.

[85] HU Q, NIU J, ZHANG K-Q, YAO M. One-Dimensional CdS/SrTiO3/Carbon Fiber Core–Shell Photocatalysts for Enhanced Photocatalytic Hydrogen Evolution [J]. Coatings, 2022, 12(9): 1235 doi: https://doi.org/10.3390/coatings12091235.

[86] TIEN T-M, CHUNG Y-J, HUANG C-T, CHEN E L. Fabrication of WS2/WSe2 Z-Scheme Nano-Heterostructure for Efficient Photocatalytic Hydrogen Production and Removal of Congo Red under Visible Light [J]. Catalysts, 2022, 12(8): 852 doi: https://doi.org/10.3390/catal12080852.

[87] DOMíNGUEZ-ARVIZU J L, JIMéNEZ-MIRAMONTES J A, HERNáNDEZ-MAJALCA B C, VALENZUELA-CASTRO G E, GAXIOLA-CEBREROS F A, SALINAS-GUTIéRREZ J M, COLLINS-MARTíNEZ V, LóPEZ-ORTIZ A. Study of NiFe2O4/Cu2O p-n heterojunctions for hydrogen production by photocatalytic water splitting with visible light [J]. Journal of Materials Research and Technology, 2022, 21: 4184-4199 doi: https://doi.org/10.1016/j.jmrt.2022.11.026.

[88] HU N, CAI Y, LI L, WANG X, GAO J. Amino-Functionalized Titanium Based Metal-Organic Framework for Photocatalytic Hydrogen Production [J]. Molecules, 2022, 27(13): 4241 doi: https://doi.org/10.3390/molecules27134241.

[89] WANG J, SHI Y, SUN H, SHI W, GUO F. Fabrication of Bi4Ti3O12/ZnIn2S4 S-scheme heterojunction for achieving efficient photocatalytic hydrogen production [J]. Journal of Alloys and Compounds, 2023, 930: 167450 doi: https://doi.org/10.1016/j.jallcom.2022.167450.

[90] TIEN T-M, CHEN E L. A Novel ZnO/Co3O4 Nanoparticle for Enhanced Photocatalytic Hydrogen Evolution under Visible Light Irradiation [J]. Catalysts, 2023, 13(5): 852 doi: https://doi.org/10.3390/catal13050852.